Progress In Electromagnetics Research Letters, Vol. 83, 65–70, 2019

Nonlinear Distortion Correction for Single Pixel Conical Scanning Radiometric Imaging System at W-Band

Xuan Lu[1, *], Zelong Xiao[2], and Taiyang Hu[2]

Abstract—Conical scanning radiometric imaging system is good at large field view but suffers from visual nonlinear distortion. The distortion is caused by azimuth and elevation sampling in sphere coordinate, especially for short range and large views. An outdoor experiment is carried out on a building, and the raw image is obtained with obvious distortion. The key to correct distortion is solving the range in relationship between sphere coordinate and Cartesian coordinate. For a specific building, it is approximately treated as a plane object, and its height is assumed known to solve the range and parameters for plane fitting. Once the coordinates of all pixels are determined, the object is represented in Cartesian coordinate, and the nonlinear distortion is corrected. If any size information for object is unknown, an arbitrary plane is also competent for distortion correction. The difference is that the correcting result is a projection onto this plane instead of real location. However, the projection is also compatible with human vision.

1. INTRODUCTION

Passive detecting techniques perform better than active techniques in covertness, as they do not transmit waves. The contradiction is well balanced between resolution and penetration capabilities within millimeter wave (MMW) band [1, 2]. Thus radiometric MMW imaging systems have been successfully used in navigation, surveillance, and homeland security of concealed weapon detection (CWD) applications [3–5]. At recent stage of MMW device development, multi-channel radiometer such as phased array or focal plane array(FPA) is still costly [6–8]. Therefore, mechanical scanning remains one of the most popular radiometric imaging approaches [9, 10]. Compared with plane scanning, conical scanning is processed in spherical coordinate. In detail, the sensor is scanned in azimuth and elevation dimensions, by which large imaging field could be viewed easily without track of big size. However, conical scanning suffers from space unevenness during sampling, even if azimuth and elevation are both equally spaced. This unevenness would lead to visual nonlinear distortion without image postprocessing, especially for large view imaging at short range.

In previous work [11–13], we fixed a single pixel conical scanning radiometric imaging system at W-band. The scanning platform supports a maximum azimuth range of -170° to 170° and a maximum elevation range of -75° to 75°, covering almost the whole space. In Section 2, the cause of nonlinear distortion for conical scanning imaging system is explained. Outdoor experiments were carried out for large view imaging, and the distortion is corrected in Section 3.1, which is followed by conclusion.

Received 18 January 2019, Accepted 19 March 2019, Scheduled 29 March 2019

* Corresponding author: Xuan Lu (xuanlu@sxu.edu.cn).

[1] Department of Electronic Information Engineering, Shanxi University, Taiyuan 030006, China. [2] School of Electronic and Optical Engineering, Nanjing University of Science and Technology, Nanjing 210094, China.

2. SINGLE PIXEL CONICAL SCANNING RADIOMETRIC IMAGING SYSTEM AT W-BAND

2.1. System Structure

The structure of our radiometric imaging system is shown in Fig. 1. The single pixel radiometer is of total power direct detection mode and works at center frequency of 94.5 GHz with bandwidth of 2 GHz. It is assembled with a Cassegrain antenna of 150 mm aperture and mounted on a conical scanning platform. The scanning platform is driven by two motors, responsible for azimuth and elevation rotations, respectively. The raw data of the radiometer are collected by a commercial ADC and transferred to industrial personal computer (IPC) by PCI interface. Scanning parameters including scanning range and speed can be set up in supporting software with GUI, and these instructions are sent to scanning platform by RS232 interface.

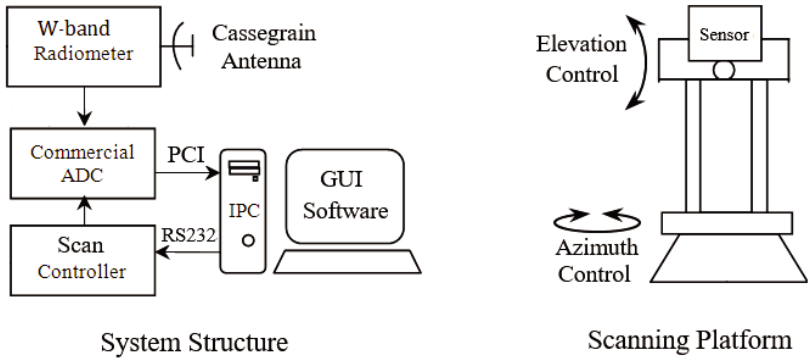

Figure 1. System Structure and the scanning platform of the radiometric MMW imaging system.

2.2. Nonlinear Distortion with Conical Scanning

Point in spherical coordinate is expressed as (R, ϕ, θ), where R indicates its range to origin, ϕ the azimuth angle, and θ the elevation angle. During conical scanning, the field of view is generally evenly sampled in azimuth and elevation dimensions because of realizability. At each sampling point (ϕ, θ), radiometric temperature is recorded as a pixel of the raw image, and the distance between adjacent pixels is $Rd\theta d\phi$ at the range of R. It implies that the absolute spatial sampling spacing relies on ϕ and θ and is heterogeneous. According to the relationship between sphere coordinate and Cartesian coordinate in Eq. (1),

$$\begin{cases} x = R\sin\theta\cos\phi \\ y = R\sin\theta\sin\phi \\ z = R\cos\theta \end{cases}, \tag{1}$$

where $R = \sqrt{x^2 + y^2 + z^2}$, and the azimuth and elevation for point (x, y, z) in Cartesian coordinate are

$$\begin{cases} \theta = \pi/2 - \arctan\dfrac{z}{\sqrt{x^2 + y^2}} \\ \phi = \arcsin\dfrac{y}{z\tan\theta} \end{cases}, \tag{2}$$

Considering that a flat rectangle object is imaged and assuming that it is located in xoz plane at $y = Y$ for example, the images of the object sampled by plane scanning and conical scanning will be in shapes as shown in Fig. 2, respectively. Compared to plane scanning, a visual difference results in conical scanning, i.e., the nonlinear distortion.

There is another problem for conical scanning radiometric imaging system besides nonlinear distortion. For a round object of diameter r, its solid angle to the sensor is $\arcsin(r/R)$ when $r \ll R$. It means that the size of the object image is related to the range as shown in Fig. 3.

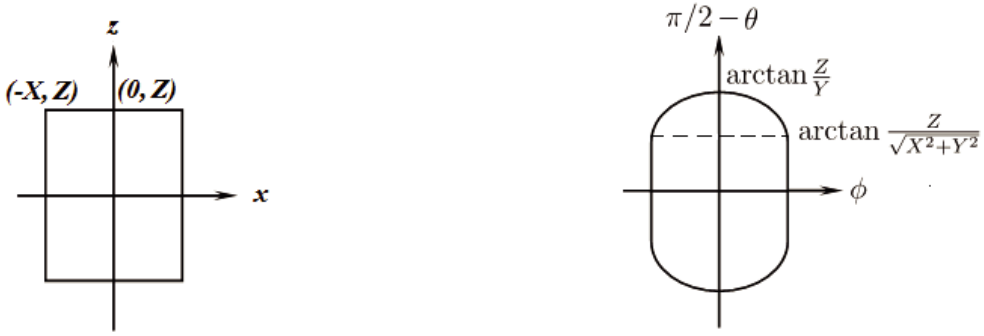

(a) Image sampled in x–z dimensions (b) Image sampled in ϕ–θ dimensions

Figure 2. Image comparison between plane scanning and conical scanning.

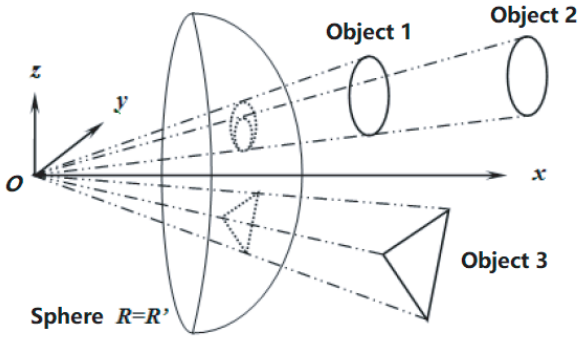

Figure 3. Different image sizes of Object 1 and Object 2 caused by conical scanning.

3. OUT DOOR EXPERIMENT AND NONLINEAR DISTORTION CORRECTION

3.1. Outdoor Experiment

In this section, outdoor experiments were carried out to simulate surveillance application. For a Cassegrain antenna of a 150 mm aperture working at 94.5 GHz, the detecting range that satisfies far field (Fraunhofer field) condition is about 14.2 m according to Eq. (3).

$$R = 2D^2/\lambda. \tag{3}$$

In the far field region, -3 dB beamwidth of the circular aperture antenna is approximately calculated as

$$\theta_{3\,\mathrm{dB}} = 1.22\lambda/D \times 180^\circ/\pi, \tag{4}$$

which is 1.5° for our antenna.

Because the nonlinear distortion is especially visualized for large view imaging at short range, we choose a building shown in Fig. 4(a) as measuring object. Several reasons are considered: 1) it is a big object with a basically flat surface; 2) the view includes typical targets such as sky, metal, and concrete material for radiometric measuring at MMW band; 3) detecting range can be easily set up. Fig. 4(b) shows the radiometric raw image measured at 15 m, a bit further than Fraunhofer field condition.

The azimuth is ranged from -40° to 30°, stepped by 0.1°, while the elevation angle is from 40° to 80° with a step of 0.5° to save imaging time. Both of the steps satisfy Nyquist′s space sampling theorem. In the image it is seen that:

(1) A cold sky background is obtained on sunny days at Spot 1, with the lowest radiometric temperature of ~ 50 K.

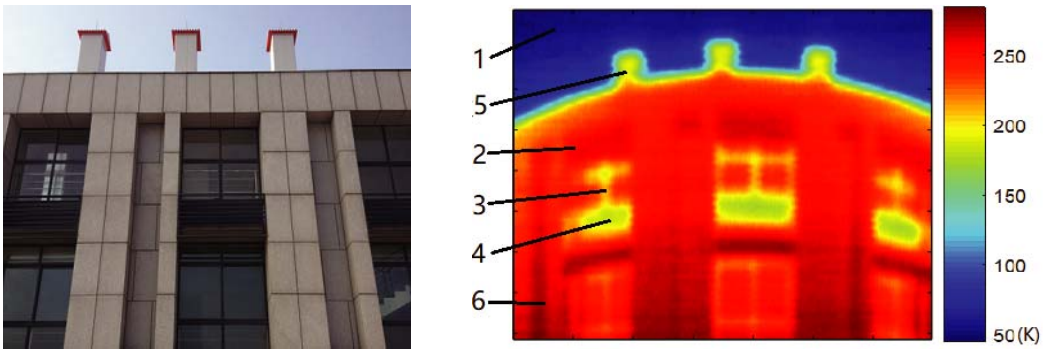

(a) Optical Photo of the view (b) Radiometric raw image

Figure 4. Outdoor experiment and results.

(2) On the contrary, the concrete wall at Spot 2 appears to have the highest radiometric temperature of $\sim 250\,\mathrm{K}$ due to a low reflectivity.

(3) The window frame at Spot 3 stands out against the concrete background with a lower temperature, as the smooth metal surface almost reflects the cold sky radiation completely. The width of the frame is about 5 cm, but the diameter of the projection of the antenna main lobe at 15 m is about $15\,\mathrm{m} \times 1.5^\circ \times \pi/180^\circ = 0.39\,\mathrm{m}$. As a result, when the window frame is swept, the high temperature of the concrete wall is weighted in the main lobe. Therefore, the radiometric temperature at Spot 3 is much higher than the sky temperature and also higher than that at Spot 4 with more metallic stuff. This weighting effect is also obvious at Spot 5 and all the other edges, which is indeed the reason for lower resolution than optical photos.

(4) As the elevation angle decreases, the radiometric temperature of the building increases because the sky temperature gets higher at large zenith angles. That is why the temperature at Spot 6 is higher than that at Spot 2.

(5) The building is distorted compared to human vision. The distortion is caused by conical scanning which has a certain relationship with Cartesian coordinate and is correctable.

3.2. Nonlinear Distortion Correction

If the coordinates of all the pixels in the raw image, (x, y, z), are certain or scaled by a constant, the distortion is corrected. Pixels in sphere coordinate can be transferred into Cartesian coordinate by Eq. (1), in which θ and ϕ are decided by pixel index and scanning range and step. However, measuring R is incapable for monocular passive sensor. In the special situation of our experiment, the building is approximated as a plane object. Assume that it belongs to a plane in general equation of $Ax + By + Cz = D$, where A, B, C, and D are parameters. As the plane is parallel to z-axis, parameter C degenerates to 0. Combining Eq. (1), if parameters A, B, and D are known, R can be calculated as

$$R = \frac{D}{A\sin\theta\cos\phi + B\sin\theta\sin\phi} \tag{5}$$

To solve A, B, and D, at least three points in the plane should be known for their coordinates. Priori knowledge of the object is quite beneficial for parameter solution. At our stage, the height of the building is the most apparent feature, which can be easily measured or estimated in other ways. It is 7 m to the ground, while the height of the sensor is 1.95 m. Therefore, the z-axis coordinate of the roof is 5.05 in Cartesian coordinate centered on the radiometer. However, it is difficult to locate the roof in radiometric image due to its low resolution, and an edge detection is performed by canny operator. The result of the edge detection is shown in Fig. 5(a). Four pixels are marked for parameter fitting of the plane equation. Their azimuth and elevation angles are respectively $(-32.7^\circ, 50^\circ)$, $(-12.4^\circ, 47.5^\circ)$, $(4.1^\circ, 48.0^\circ)$ and $(22.3^\circ, 51.5^\circ)$, and the fitted plane is $7.2x + y = 118.5$. The ranges of all the pixels can be calculated according to Eq. (5). Since (R, ϕ, θ) for all pixels are determined, the object can

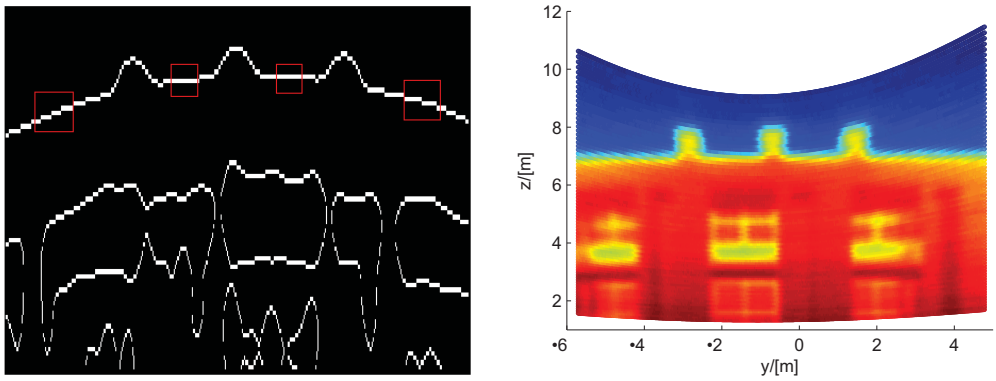

(a) Edge detection result by canny operator

(b) The front view of the building

Figure 5. Distortion correcting result.

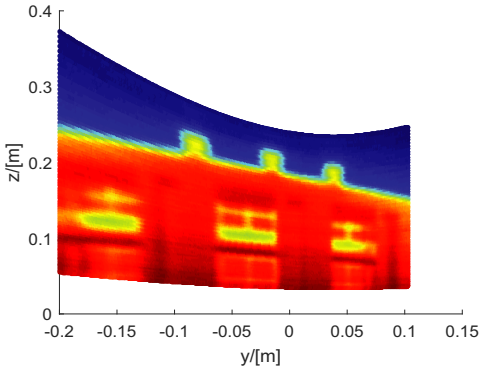

Figure 6. Correcting result with an arbitrary plane $5x + y = 1$.

be represented in Cartesian coordinate. A front view of the building is shown in Fig. 5(b), in which: 1) the distortion is corrected; 2) the origin has been converted to the ground, and it is seen that the building is of 7 meters high; 3) during coordinate conversion, a rectangle area in the raw image becomes a curved-edge shape, but only the center of the area is calculated. While displaying the corrected image, the calculated centers will act as pixels and stand for rectangle areas which cannot fill up the field with curved-edge shapes. In case whitespace between pixels appears, filled circles are chosen for pixel markers. Big markers lead to overlap in pixel-dense region such as the building in this occasion, while small markers will cause whitespace in pixel-sparse region like top right corner of the image.

Indeed, the picture below the roof curve can compress each column of pixels into equal height to get a rectangle. Similarly, the part above the curve can be stretched into a rectangle. If any size information for object is unknown, or the plane equation of the object cannot be solved, an arbitrary plane is competent to calculate pixel coordinate. The result of (R', ϕ, θ) represents object projection onto this plane. Fig. 6 shows a result with plane $5x + y = 1$. It can be seen that the projection is compatible with human vision. And it is also applicable to stereo objects.

4. CONCLUSION

This paper proposes a nonlinear distortion correcting approach for single pixel conical scanning radiometric imaging system at W-band. Conical scanning views large field by azimuth and elevation sampling. But the raw image is incompatible with human vision because spherical coordinate is nonlinear, especially for large view at short range. Regardless of the vibration and noise during scanning, the distortion is known by relationship between sphere coordinate and Cartesian coordinate.

In coordinate transferring, solving R is critical, and the characteristic of the object is beneficial. Even if no prior knowledge is known about the object, a projection onto an arbitrary plane can be calculated, which is compatible with human vision.

ACKNOWLEDGMENT

This work is supported by 2018 Shanxi Provincial Startup Foundation for Advanced Talents (No. 127545004).

REFERENCES

1. Yujiri, L., "Passive millimeter wave imaging," *2006 IEEE MTT-S International Microwave Symposium Digest*, 98–101, 2006.
2. Appleby, R., "Passive millimetre-wave imaging and how it differs from terahertz imaging," *Philosophical Transactions of the Royal Society of London Series a Mathematical Physical and Engineering Sciences*, Vol. 362, 379–392, 2004.
3. Viegas, C., B. Alderman, J. Powell, H. Liu, H. Wang, and R. Sloan, "Millimeter wave radiometers for applications in imaging and nondestructive testing," *8th UK, Europe, China Millimeter Waves and THz Technology Workshop (UCMMT)*, 1–4, 2015.
4. Isiker, H., C. Ozdemir, and I. Unal, "Millimeter-wave band radiometric imaging experiments for the detection of concealed objects," *2015 IEEE Radar Conference*, 23–26, 2015.
5. Chen, H.-M., S. Lee, R. M. Rao, M. A. Slamani, and P. K. Varshney, "Imaging for concealed weapon detection: a tutorial overview of development in imaging sensors and processing," *IEEE Signal Processing Magazine*, Vol. 22, No. 2, 52–61, 2005.
6. Cui, G., C. Zhao, H. Wu, X. Wei, and Z. Li, "Millimeter wave passive imaging system using reflector antenna," *2015 IET International Radar Conference*, 1–5, 2015.
7. Wang, W., A. E. Fathy, and X. Wang, "Novel antenna using substrate integrated waveguide for passive millimeter-wave focal plane array imaging," *2014 IEEE International Wireless Symposium*, 1–4, 2014.
8. Lukin, K. A., et al., "Coherent radiometric imaging in range-azimuth plane using antennas with beam synthesizing," *11th European Radar Conference*, 45–48, 2014.
9. Lee, D., S. Yeom, J. Son, and S. Kim, "Image segmentation of concealed objects detected by passive millimeter wave imaging," *2009 34th International Conference on Infrared, Millimeter, and Terahertz Waves*, 1–2, 2009.
10. Kholmatov, A., et al., "Passive millimeter-wave band data acquisition setup and associated image processing techniques," *21st Signal Processing and Communications Applications Conference (SIU)*, 1–4, 2013.
11. Lu, X., Z. Xiao, J. Xu, and H. Huo, "3D millimeter wave image by combined active and passive system," *Progress In Electromagnetics Research L*, Vol. 50, 7–12, 2014.
12. Lu, X., F. Peng, G. Li, Z. Xiao, and T. Hu, "Object segmentation for linearly polarimetric passive millimeter wave images based on principal component analysis," *Progress In Electromagnetics Research M*, Vol. 61, 169–176, 2017.
13. Lu, X., Z. Xiao, and J. Xu, "Linear polarization characteristics for terrain identification at millimeter wave band," *Chinese Optics Letters*, Vol. 12, No. 10, 1012011–1012015, 2014.